Ecological Indicators 67 (2016) 637–648

Contents lists available at ScienceDirect

Ecological Indicators

journal homepage: www.elsevier.com/locate/ecolind

Remote estimation of canopy height and aboveground biomass of maize using high-resolution stereo images from a low-cost unmanned aerial vehicle system

Wang Li [a,*], Zheng Niu [a], Hanyue Chen [b,*], Dong Li [c], Mingquan Wu [a], Wei Zhao [a]

[a] The State Key Laboratory of Remote Sensing Science, Institute of Remote Sensing and Digital Earth, Chinese Academy of Sciences, Beijing 100101, China
[b] College of Resource and Environmental Science, Fujian Agriculture and Forestry University, Fuzhou 350002, China
[c] Airborne Remote Sensing Center, Institute of Remote Sensing and Digital Earth, Chinese Academy of Sciences, Beijing 100101, China

ARTICLE INFO

Article history:
Received 1 December 2015
Received in revised form 16 February 2016
Accepted 17 March 2016
Available online 25 April 2016

Keywords:
Unmanned aerial vehicle
Stereo images
Point clouds
Canopy height
Maize biomass

ABSTRACT

Canopy height (H_{canopy}) and aboveground biomass (AGB) of crops are two basic agro-ecological indicators that can provide important indications on the growth, light use efficiency, and carbon stocks in agro-ecosystems. In this study, hundreds of stereo images with very high resolution were collected to estimate H_{canopy} and AGB of maize using a low-cost unmanned aerial vehicle (UAV) system. Millions of point clouds that are related to the structure from motion (SfM) were produced from the UAV stereo images through a photogrammetric workflow. Metrics that are commonly used in airborne laser scanning (ALS) were calculated from the SfM point clouds and were tested in the estimation of maize parameters for the first time. In addition, the commonly used spectral vegetation indices calculated from the UAV orthorectified image were also tested. Estimation models were established based on the UAV variables and field measurements with cross validation, during which the performance of the UAV variables was quantified. Finally, the following results were achieved: (1) the spatial patterns of maize H_{canopy} and AGB were predicted by a multiple stepwise linear (SWL) regression model (R^2 = 0.88, rRMSE = 6.40%) and a random forest regression (RF) model (R^2 = 0.78, rRMSE = 16.66%), respectively. (2) The UAV-estimated maize parameters were proved to be comparable to the field measurements with a mean error (ME) of 0.11 m for H_{canopy}, and 0.05 kg/m^2 for AGB. (3) The SfM point metrics, especially the mean point height (H_{mean}) greatly contributed to the estimation model of maize H_{canopy} and AGB, which can be promising indicators in the detection of maize biophysical parameters. To conclude, the variations in spectral and structural attributes for maize canopy should be simultaneously considered when only simple RGB images are available for estimating maize AGB. This study provides some suggestions on how to make full use of the low-cost and high-resolution UAV stereo images in precision agro-ecological applications and management.

1. Introduction

Canopy height (H_{canopy}) and aboveground biomass (AGB) of crops are two basic agro-ecological indicators for the study of environmental processes and precision agriculture. The H_{canopy} and AGB of crops provide important indications on the growth, light use efficiency, and carbon stocks in agro-ecosystems (Li et al., 2015a), which are closely related to the yield production and human living. A rapid, economical and quantitative estimation of crop biomass is important for accessibility risk management, global markets, policy-making, and decision-making (Becker-Reshef et al., 2010). The most direct way quantitatively to capture the values of crop height and biomass is to measure the plant height by tape and to oven dry the plants to constant weight by destructive harvest, respectively. Thus, it is challenging and time consuming for ecologists and agronomists to conduct long-term measurements of crop height and biomass over large-scale areas.

In recent decades, remote sensing has gained weight in the estimation of large-scale distributions of crop biophysical parameters due to its ability to collect non-destructive multi-temporal information at regional and global scales. Satisfactory relationships have been found between the remotely sensed spectral variables

* Corresponding authors at: The State Key Laboratory of Remote Sensing Science, Institute of Remote Sensing and Digital Earth, Chinese Academy of Sciences, P.O. Box 9718, No. 20 Datun Road, Olympic Science & Technology Park of CAS, Beijing 100101, China. Tel.: +86 010 64889215; fax: +86 010 64889215.
E-mail addresses: lwwhdz@sina.com (W. Li), chenhanyue.420@163.com (H. Chen).

http://dx.doi.org/10.1016/j.ecolind.2016.03.036
1470-160X/

and vegetation parameters such as phenology indicators (Gonsamo et al., 2013; Wu and Chen, 2013), light use efficiency (Wu et al., 2012), leaf area index (LAI) (Kross et al., 2015), and AGB (Coltri et al., 2013; Liu et al., 2010). Nevertheless, the spectral signals of remotely sensed images tend to saturate with vegetation biomass in areas with dense canopies. In addition, most satellite-based images can hardly provide the vertical structure information of vegetation canopy. To obtain the vertical height of vegetation, photogrammetric techniques have been developed and applied to groups of stereo images (Ni et al., 2014, 2015). However, it is costly and difficult to acquire so many satellite-based stereo images, because the visiting cycle of most open-access satellite data is too long for photogrammetric analysis. The later-presented airborne laser scanning (ALS) or light detection and ranging (LiDAR) technique helped to overcome the saturation problem because of its high penetration capability. The layered features of vegetation canopy like plant height can be directly obtained from the returned laser signals. Both airborne and terrestrial laser scanning (TLS) systems have been widely employed in the study of forest vegetation (Höfle et al., 2012; Hyyppa et al., 2012; Listopad et al., 2015). As the growth status of crops varies a lot during the growing season compared with forest, the TLS system is preferred in the multi-temporal monitoring of crops because it is more cost efficient. Detailed geo-information of crops like maize, whose canopy height is short can be provided by TLS even at the individual plant level (Höfle, 2014). Despite the high cost, the ALS data were proved to have great potential in estimating the canopy height and biomass of maize in the peak growing season based on our previous studies, and the estimated error varied from 0.15 to 0.17 m for H_{canopy}, and 0.29–0.49 kg/m^2 for AGB (Li et al., 2015a,c). In addition, the full-waveform of ALS has been proved to be more powerful in the height extraction of maize height compared with discrete point clouds (Gao et al., 2015). This is important for large-scale monitoring of precision farming as ALS can provide a larger measuring scale than TLS. However, ALS tends to overestimate canopy LAI and underestimate canopy height especially for short vegetation types like maize (Li et al., 2015a). In addition, both ALS and TLS datasets are difficult to acquire in terms of practicality and cost for vegetation detection, because repeat acquisitions are usually needed with an increased cost (Mathews and Jensen, 2013; Omasa et al., 2007). The point density of ALS data can be significantly increased with repeat airborne flights, giving a better description of the interactions between laser pulses and targets.

The recent advent of unmanned aerial vehicles (UAVs) seems to be a promising trade-off between airborne and terrestrial remote sensing in the study of precision agriculture and ecological management. Compared with manned airborne and terrestrial systems, an evident advantage of UAV systems is that they can work at low flight heights that are close to the targets with no risk to human life in different and inaccessible areas. In addition, it can provide a much larger ranging scope than TLS. The low cost and high flexibility have led to UAV systems rapidly being employed in agriculture (Geipel et al., 2014; Link et al., 2013) and forestry management (Getzin et al., 2014; Jaakkola et al., 2010). Detailed discussions on the evolution and state-of-the-art of the use of UAV systems have been reviewed by Colomina and Molina (2014). Both imaging and non-imaging sensors can be mounted on a small UAV, providing various types of remotely sensed data (Aasen et al., 2015). Hundreds of images with centimeter spatial resolution can be collected by a small and lightweight UAV system controlled by pre-programmed flying plans (Lisein et al., 2013), which can be used for applications at different scales. The structure of motion (SfM) technique has been proved to be a very efficient approach to organize and process the many overlapped UAV images based on the principles of photogrammetry. The SfM approach greatly improved the automation of the photogrammetric workflow so that very dense point clouds at sub-pixel accuracy can be produced in near real-time at low cost (Leberl et al., 2010). The SfM point clouds are usually of much higher point density than ALS and TLS, which is important for precision study of vegetation structure. Most of the previous studies of vegetation based on UAV mainly focused on the application of three-dimensional digital models and the spectral variables including the raw digital numbers and vegetation indices (VIs) (Aasen et al., 2015; Bendig et al., 2015; Candiago et al., 2015). However, considerably fewer studies explored the direct use of SfM point clouds. According to Mathews and Jensen (2013), metrics generated from the SfM point clouds (point heights, number of points, etc.) can be efficiently used to predict the canopy LAI of vineyard vegetation. In fact, these types of metrics calculated from ALS point clouds have been used in estimating biophysical parameters of vegetation (Li et al., 2015b; Luo et al., 2015). Comparisons on the similarities and differences between ALS and UAV SfM point clouds have been conducted on the extraction of forest inventory attributes (White et al., 2013). For the UAV detection of maize, spectral VIs calculated from the RGB color space have been used as the main proxies to predict maize parameters (Liebisch et al., 2015; Pena et al., 2013; Zaman-Allah et al., 2015). This is probably because of the good responses of biophysical and biochemical canopy components to solar radiation at different spectral wavelengths. To the best of our knowledge, few studies have employed or compared the ability of the SfM point cloud metrics in the estimates of maize biomass for the same dataset. In addition, the contribution and performance of different types of UAV variables during the estimation still need quantitative evaluation. With the rapid advent of UAV data, we believe that the SfM point cloud metrics will be widely used in future estimations of vegetation parameters.

Therefore, this study aimed to further explore the UAV detection of two maize parameters, namely, H_{canopy} and AGB. In addition to the spectral VIs, ALS-similar metrics were also calculated from the UAV SfM point clouds (denoted as SfM point metrics hereafter). It is expected that the addition of these point metrics will help to increase the estimation accuracy of maize parameters. The performance and contribution of these SfM point metrics and the spectral VIs were tested and quantified in the estimation of maize parameters. Estimation models were established and cross-validated by field measurements, and were further used to predict the spatial patterns of maize parameters. Based on the analysis in this study, we hope to provide some suggestions on how to make full use of the low-cost and high-resolution UAV stereo images in precision agro-ecological applications and management.

2. Materials

2.1. Study site

The study site called Huailai area is located in the Huailai-Yanqing Basin with a quite flat terrain, along the south of Guanting Reservoir, 84 km north of Beijing, China. Maize is the dominant crop type in this area, usually sowed in late May, flowering near late July, and harvested between middle and late September (Gao et al., 2013). The mean elevation is 30 m above sea level, and the mean annual temperature is 9.1 °C with the coldest temperature in January and the hottest in July. Precipitation is distributed unevenly in the four seasons with an average annual precipitation of 396 mm, the greatest precipitation occurring in summer.

2.2. UAV flight and data processing

The UAV flights were conducted on August 9, 2015. Detailed flight plans were made before data acquisition. A multiple rotor-wing UAV system was used for the collection of stereo images with an overlap set to 80% longitudinal and 40% lateral. The UAV platform

Table 1
Basic statistics of the point density in the field plots, edge, and nonedge part of the study site.

Point Density	Plot	Edge part	Non-edge part
Min	264.70	30.15	1322.83
Max	4033.28	1044.65	4149.82
Mean	2399.00	455.44	3050.03
SD	1088.17	412.73	839.70
CV	45.36%	90.62%	27.53%

Min is minimum value, Max is maximum value, Mean is mean value, SD is standard deviation, CV is coefficient of variation.

was equipped with two SONYA6000 cameras and a global positioning system (GPS) as the payload. It has a maximum flight time of 30 min under optimal weather conditions. The flight height for the UAV was set to 150 m above ground level. Thus, the ground sampling distance was 0.02 m with an estimated field of view of 300 m × 300 m. The camera has a focal length of 20 mm and produces images in three bands that spectrally suitable for vegetation detection, namely, red (R, 625 nm), green (G, 550 nm), and blue band (B, 485 nm). During the UAV flight, the camera was set with predefined settings and a shutter speed of 1/1000 s, ensuring the best exposure and not being affected by motion. The GPS load on the UAV platform can only provide rough positions; therefore, 26 ground control points (GCPs) were marked and positioned using a Trimble GeoXH differential global positioning system (DGPS) with a mean estimated error of 0.1 m within the UAV flight extent (Fig. 1(a)). About 894 images with a size of 6000 × 4000 pixels were collected. Then, stereo images were geometrically corrected using the geographic information of GCPs during the photogrammetric workflow. The locations of the GCPs were positioned according to the same base station of coordinate system as the previous ALS campaign in July 2014 (Li et al., 2015c). The base station was precisely positioned based on a permanent benchmark that is located in the Huailai station. This makes it possible to use directly the ALS-derived digital elevation model (DEM) to normalize the elevation of SfM point clouds without geographic registration. The height accuracy of DEM was assessed using GPS points with a height error of 0.05 ± 0.12 m (Nie et al., 2016), which is accurate enough to capture the normalized height.

The Smart3DCapture software was used to generate the ALS-similar point clouds with RGB color information. First, auto aerial triangulation was conducted based on the UAV stereo images. The SfM point clouds were geo-referenced using the accurate geographic information from the 26 GCPs. Second, a high densification was set to automatically produce the SfM point clouds. Outliers that were much higher or lower than other points in the point clouds were manually removed. The spatial extent of the dataset was slightly reduced by removing some distortions in the flight boundary. The point density varied significantly in different parts of the study site due to the different number of stereo images especially in the edge part of the study site (coefficient of variation, CV = 90.62%). The average point density was 2399.00 pts/m^2 for the field plots, 455.44 pts/m^2 for the edge part, and 3050.03 pts/m^2 for the non-edge part (Table 1). As the SfM point clouds were generated from the stereo images, they can only provide signals returned from the canopy surface. The elevation of the point clouds was normalized using the ground information from the ALS-derived DEM, which was further used to interpolate the digital surface model (DSM) with a pixel size of 0.2 m. Then, the DSM and orthorectified image were generated based on the point clouds. For the maize areas, the difference between DSM and DEM was calculated as the canopy height model (CHM) or crop surface model (CSM). Finally, the SfM point clouds with RGB color information and corresponding DSM were exported in the reference frame WGS84 and in the geographic map projection UTM (zone 50 N).

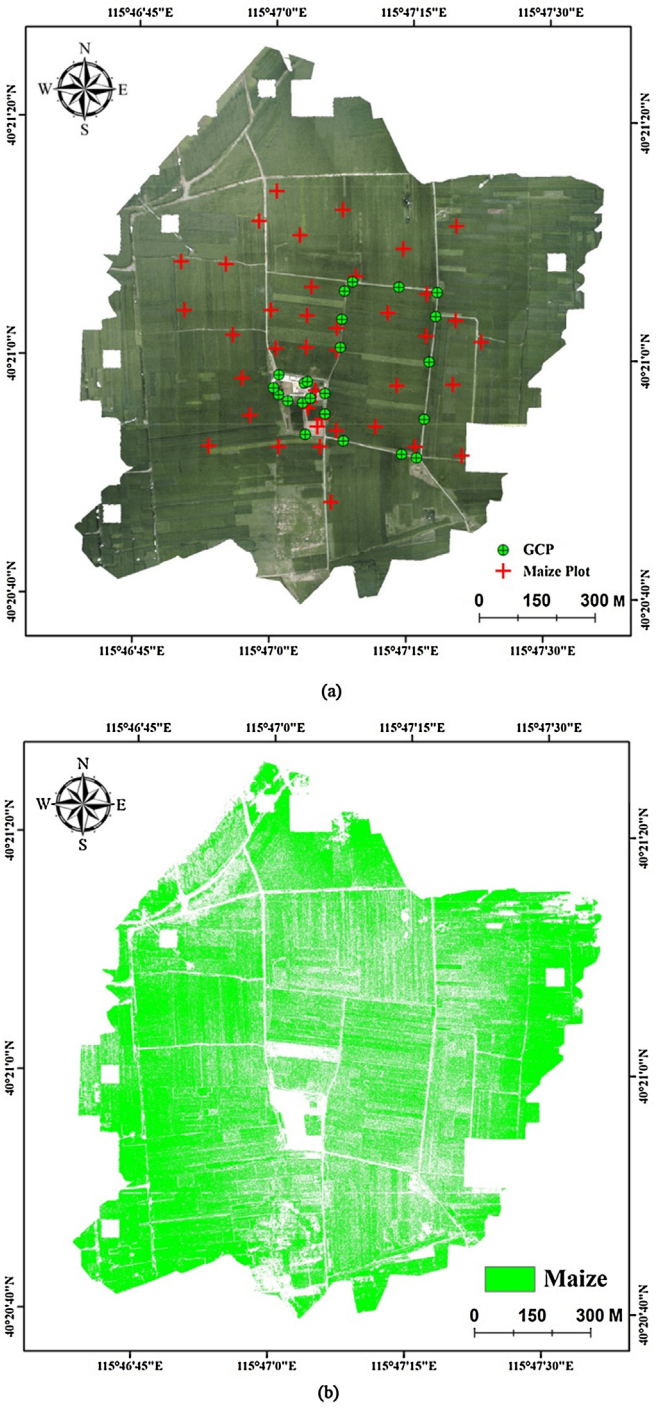

Fig. 1. The orthorectified image produced from the UAV flight in Huailai area with (a) ground control points (GCPs), and field plots of maize overlaid; (b) the classification map of maize cover obtained by the model of decision tree.

2.3. Field measurements

Field measurements were conducted three days after the UAV flights. There were 37 field plots of maize were subjectively selected by referring to the UAV orthorectified image (Fig. 1(a)). Relatively large differences among the plots were considered, resulting from different fertilization and irrigation throughout the growing season. Each field plot has a large area, flat terrain, and maize under uniform growing conditions. The geographic locations (latitude and longitude) of all the plots were positioned using a GPS. In each

Table 2
Basic statistics of the field-measured plant density (D, plant/m^2), canopy height (H_{canopy}, m) and aboveground biomass (AGB, kg/m^2) of maize.

	D (plant/m^2)	H_{canopy} (m)	AGB (kg/m^2)
N	37	37	37
Min	4.35	1.58	0.79
Max	9.70	3.64	2.63
Mean	6.01	2.46	1.65
SD	1.27	0.47	0.48
CV	21.18%	19.11%	24.80%

N is the number of plots.

plot, the heights of four representative maize plants were measured using a tape. H_{canopy} for each plot was calculated as the average height (m) of the measured maize plants. Plant density (D, plant/m^2) was determined according to the measured interplant row and line distances (m). Thereafter, two to three representative maize plants were harvested by cutting the whole plant from the bottom on the ground. The harvested plants were then sealed in a plastic bag and immediately transported to a nearby laboratory for subsequent analysis. The harvested fresh maize plants were oven dried at 85 °C until their mass reached a constant weight. Thereafter, AGB (kg/m^2) for each plot was calculated as the product of average dry weight per plant (W_{plant}, kg/plant) and the average plant density of maize (D, plant/m^2). Based on the field measurements of 37 maize plots (Table 2), the maize AGB showed a larger spatial variability than H_{canopy} with a higher CV (24.80% > 19.11%). The average plant density for all the plots was 6.01 plant/m^2 (CV = 21.18%). The field plots obtained a mean value of 2.46 m for H_{canopy} and 1.65 kg/m^2 for AGB, which corresponds to the fact that most of the maize plants were reaching the peak growing season.

3. Methodology

3.1. Calculation of UAV variables

To estimate the AGB of maize, seven previously published VIs were calculated as different mathematical combinations of the RGB digital numbers from the orthorectified image (Table 3). Most of the VIs selected in this study were greenness indices that have been proved to be powerful indicators for the estimation of vegetation fraction (Torres-Sánchez et al., 2014). Similar VIs have been widely developed and applied in the estimation of diverse vegetation biophysical parameters such as LAI (Gonsamo, 2010), chlorophyll content (Wu et al., 2008), as well as AGB (Tian et al., 2014). All the seven VIs can provide good indications of the spectral variability of vegetation canopies especially in the horizontal plane. Among the seven VIs, COM is the only index that is calculated as the combination of three other VIs. Because the definitions of ExG and ExGR are similar and both of them are involved in the calculation of COM, only ExG and COM were used in the subsequent analysis. In addition, ALS-similar metrics were also calculated based on the SfM point clouds with normalized heights, which are denoted as SfM point metrics hereafter. These point cloud-based metrics have been successfully employed to estimate the structural parameters and AGB of forest (Li et al., 2014; Pang and Li, 2013). In this study, we calculated five SfM point metrics including the mean of point height (H_{mean}), two percentile height metrics (H_{50} and H_{90}), the standard deviation of the point height (H_{std}), and the coefficient of point height variation (H_{cv}). Specifically, H_{mean}, H_{50} and H_{90} can directly describe the vertical distribution of canopy height at the middle and upper canopy levels while H_{std} and H_{cv} can give insights into the vertical complexity and heterogeneity of the canopy components (Li et al., 2014). Furthermore, most of these metrics calculated from ALS point clouds have been proved to have great power in the estimation of maize parameters (Li et al., 2015c). The pixel-wise UAV variables within each field plot were averaged by zonal statistics to obtain the values per plot. The performance of these metrics in the estimation of maize parameters was expected to be tested in this study. Before assessing the predictability of the UAV variables, intercorrelation and spatial variability were analyzed using Pearson's correlation coefficient (R) and the coefficient of variation (CV), respectively. To obtain the spatial patterns of the UAV variables in maize fields, the spatial distribution of UAV variables over the whole study area was overlapped with the maize classification data. Detailed demonstrations on producing the classification data of maize are given in Section 3.2.

3.2. Classification of maize cover

Classification of maize cover was conducted based on the UAV-derived raster including the normalized height of DSM, the DSM-derived slope, and green vegetation index GLA. The decision tree model was selected to distinguish maize from other types of land cover. Previous study proved that the decision tree model is a simple and fast classification approach especially in the flat terrain in this study (Li et al., 2015c). Referring to the orthorectified image,

Table 3
Definitions of the spectral vegetation indices and SfM point metrics that derived from UAV orthorectified image and point clouds.

UAV variable	Definition	Source
Spectral vegetation index		
Green leaf algorithm	$GLA = (2*G - R - B)/(2*G + R + B)$	Louhaichi et al. (2001)
Normalized green-red difference index	$NGRDI = (G - R)/(G + R)$	Gitelson et al. (2002)
Excess green index	$ExG = 2*G - R - B$	Woebbecke et al. (1995)
Excess green minus excess red index	$ExGR = ExG - 1.4R - G$	Neto (2004)
Color index of vegetation	$CIVE = 0.441*R - 0.881*G + 0.385*B + 18.78745$	Kataoka et al. (2003)
Vegetativen	$VEG = G/(R^a B^{(1-a)})\ a = 0.667$	Hague et al. (2006)
Woebbecke index	$WI = (G - B)/(R - G)$	Woebbecke et al. (1995)
Combination	$COM = 0.25*ExG + 0.3ExGR + 0.33*CIVE + 0.12*VEG$	Guijarro et al. (2011)
SfM point metric		
Mean height	$aH_{mean} = \frac{1}{N}\sum_{i=1}^{N} h_i$	–
Percentile height	$(N-1)p\% = j + g,\ p^{th} = h_j (g = 0);\ p^{th} = h_j * g + (1-g) * h_{j+1}\ (g \neq 0)$	–
Standard deviation of height	$H_{std} = \sqrt{\frac{1}{N}\sum_{i=1}^{N}(h_i - H_{mean})}$	–
Coefficient of Variation	$CV = H_{std}/H_{mean}$	–

h_i = height of point; N = number of points; p = percentiles; j = the integer part; g = fractional part.

areas of interest in different types of land cover were sampled to determine the thresholds used in the structure of the decision tree model. The normalized height from DSM was first used to separate maize and some non-vegetation from other land covers with a height threshold within 1.5–3.95 m according to the field survey of maize height. Then, the vegetation index GLA (>0.1) was set to discriminate the vegetation covers from non-vegetation cover such as low buildings and bare soil. The DSM-derived slope (<20°) was used to discriminate maize field from low vegetation in uneven areas because the maize fields in this study all possessed a flat terrain. Finally, the decision tree model was executed to obtain the classification map of maize based on the wall-to-wall UAV-derived raster. Later, manual interpretation and reclassification were conducted to correct some misclassification pixels such as the short trees located in the Huailai experiment station. The final classification result of maize is shown in Fig. 1(b).

3.3. Estimation models and validation

Before the establishment of estimation models, inter-correlation and spatial variability among all of the UAV variables were analyzed using Pearson's correlation coefficient (R) and basic statistic estimators. As the SfM point clouds can provide a direct indication of the plant heights and biomass, the maize H_{canopy} and AGB were directly evaluated using the average heights of the normalized SfM point clouds (H_{mean}) within a grid size of 2 m. Simple linear regression (SLR) models were established based on the plot-wise H_{mean} and field-measured H_{canopy} and AGB, respectively. In addition, both UAV spectral VIs and SfM metrics were used to develop the estimation models of maize H_{canopy} and AGB. The commonly used stepwise linear regression (SWL) model was first explored. To fully explore the explaining power from the combination of different UAV variables, an exhaustive search for the best subsets of UAV variables for predicting H_{canopy} and AGB in the linear regression was conducted, respectively. The subsets of variables selected by linear regression for all possible models were ordered by two measures, namely, adjusted coefficient of determination (R^2) and Bayesian information criterion (BIC). The model with the highest R^2 and lowest BIC will be taken as the final SWL model. In the interpretation of the regression model coefficients, a low p-value usually indicates a meaningful addition to the estimation model because changes in the predictor are related to changes in the response variable. Thus, the contribution made by each UAV variable to the SWL model was quantified with a p value $\leq$0.001 representing very highly significant; $0.001 < p \leq 0.01$ representing highly significant; $0.01 < p \leq 0.05$ representing significant; and otherwise representing nonsignificant. Comparisons between the parametric models (SLR and SWL) and a nonparametric model, namely the random forest (RF) regression model were conducted. To avoid over fitting and to facilitate variable selection, the variables selected by stepwise regression were further used to develop the RF model. The random forest parameters (*mtry* and *ntree*) were optimized to obtain the best predictive power during the regression. The importance of the selected variables to the RF model was quantified using the percentage increase in mean square error (IncMSE%) and total increase in node purities (IncNodePurity). The node purity was measured by residual sum of squares. More details on the mechanism of these two models and corresponding programming functions can be found in the library packages in the statistical software R (http://www.r-project.org/).

A leave-one-out cross-validation (LOOCV) method was used to assess the prediction accuracy during the estimation of H_{canopy} and AGB. The estimation accuracy was quantified using coefficient of determination (R^2), root mean square error (RMSE) (Eq. (1)) and relative root mean square error (rRMSE) (Eq. (2)). RMSE is related to the magnitude of the observed variables, while rRMSE is a relative value that can be used to compare the performance of different regression models. A lower rRMSE often indicates a better regression performance.

$$\mathrm{RMSE} = \sqrt{\frac{1}{n}\sum_{i=1}^{n}(p_i - \hat{p}_i)^2} \quad (1)$$

$$rRMSE = \frac{RMSE}{\overline{p_i}} \quad (2)$$

where p_i is the measured value and $\hat{p}_i$ is the predicted value. To examine whether there were statistically significant differences among the estimated results from different models, a one-way analysis of variance (ANOVA) at the $p < 0.05$ level was conducted with the use of the Duncan post hoc test.

4. Results

4.1. Analysis of plot-wise UAV variables

Both the spectral VIs and SfM point metrics were sampled by zonal statistics within the extent of each plot. The basic statistics of all the sampled UAV variables (Table 4) showed that the plot-wise SfM point metrics generally obtained greater spatial variability than the spectral VIs with higher CVs. Specifically, H_{std} showed the largest spatial variability (CV = 59.97%) followed by H_{cv} (CV = 53.64%). This indicated that the field plots showed a large variation of canopy complexity because H_{std} and H_{cv} are two metrics that can describe the dispersion of point clouds in the vertical direction (Li et al., 2014). The mean of plot-wise H_{cv} showed that the maize canopies in this study generally possessed moderate rugosity and complexity. Among the spectral VIs, GLA showed the highest spatial variability with a range of 0.07–0.22 (CV = 37.46%). VEG showed the smallest spatial variability among all of the UAV variables.

Results showed that high correlations were found between the field-measured H_{canopy} and the UAV variables especially the SfM point height metrics such as H_{mean} (R = 0.86) and H_{90} (R = 0.75). Nevertheless, the spectral indices showed relative lower correlations to H_{canopy} than the SfM point metrics did (Fig. 2). A generally moderate correlation was obtained for each individual variable to AGB. Among all of the UAV variables, H_{mean} showed the highest correlation with the field-measured AGB (R = 0.73) followed by NGRDI (R = 0.68) and H_{cv} (R = 0.61). Nevertheless, inter-correlation was found between several pairs of variables in either spectral type or SfM point type. For instance, the vegetation index GLA showed high correlation with VEG (R = 0.98). The height variables H_{50} and H_{90} also showed significant inter-correlation (R = 0.60). In addition,

Table 4
Basic statistics of the plot-wise spectral vegetation indices and SfM point metrics that calculated from UAV orthorectified image and point clouds, respectively.

UAV Variables	Min	Max	Mean	SD	CV
Spectral vegetation index					
CIVE	−14.90	−2.07	−8.56	2.05	−23.91%
COM	−70.61	−10.77	−35.92	8.68	−24.16%
ExG	31.00	64.00	50.86	8.39	16.49%
GLA	0.07	0.22	0.16	0.06	37.46%
NGRDI	0.05	0.16	0.11	0.04	35.08%
VEG	1.10	1.50	1.33	0.08	5.67%
SfM point metric					
H_{mean}	1.59	3.49	2.53	0.51	20.15%
H_{std}	0.08	0.94	0.37	0.22	59.97%
H_{cv}	0.05	0.22	0.12	0.06	53.64%
H_{50}	1.30	3.34	2.25	0.50	22.08%
H_{90}	1.86	3.53	2.71	0.38	14.22%

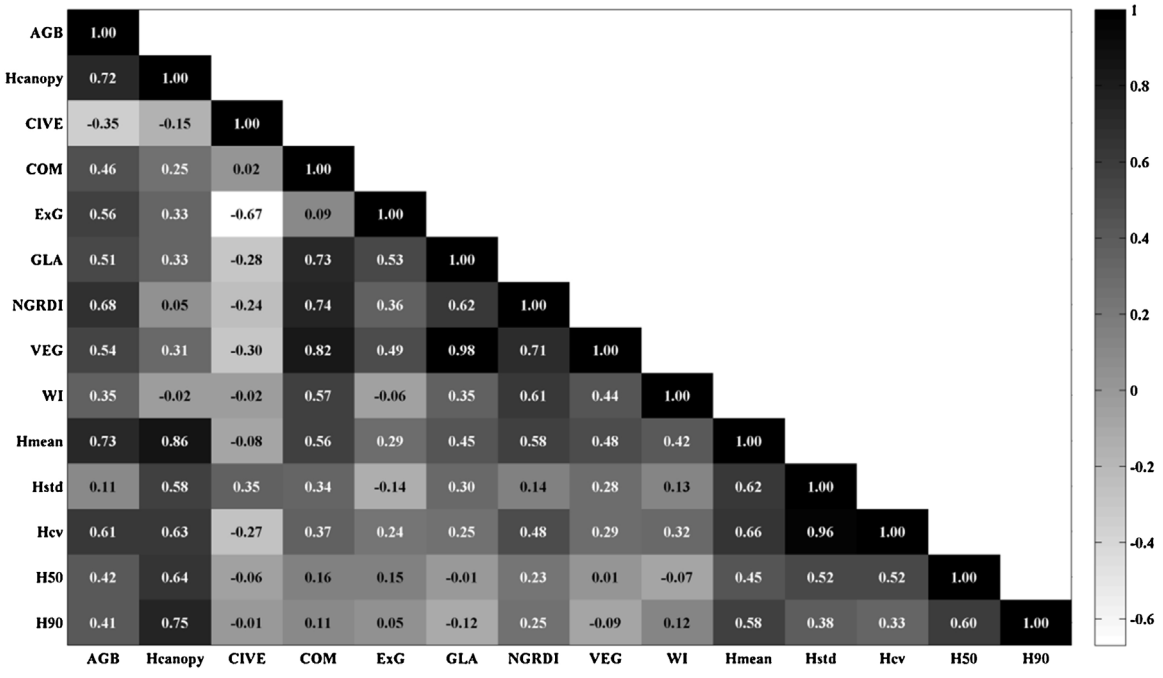

Fig. 2. Pearson's correlation (R) between maize parameters (H_{canopy} & AGB) and individual UAV variables.

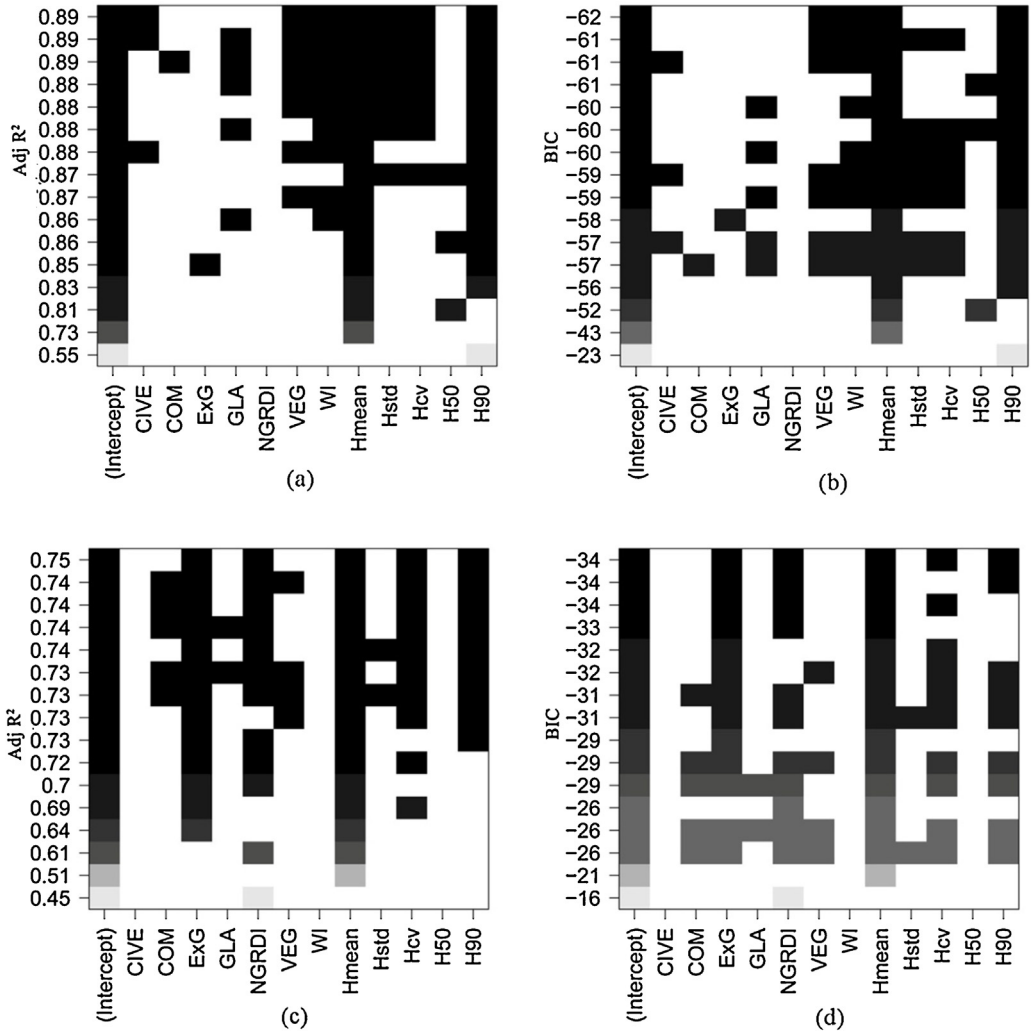

Fig. 3. Subsets of variables selected by linear regression for all possible models ordered by adjusted coefficient of determination (Adj R^2) and Bayesian information criterion (BIC) for H_{canopy} (a, c) and AGB (b, d) of maize.

Table 5
Accuracies of estimation models from LOOCV procedure for maize canopy height (H_{canopy}, m) and aboveground biomass (AGB, kg/m^2). SLR: simple linear regression model; SWL: stepwise linear regression model; RF: random forest regression model.

Model	R^2	ME	RMSE	rRMSE
H_{canopy} (m)				
SLR	0.74**	0.15	0.21	8.40%
SWL	0.88**	0.11	0.16	6.40%
RF	0.72**	−0.04	0.26	10.40%
AGB (kg/m^2)				
SLR	0.52**	0.09	0.31	18.79%
SWL	0.64**	0.16	0.35	21.11%
RF	0.78**	0.05	0.27	16.66%

** $p < 0.01$.

a generally negative correlation was found between CIVE and the other variables with the highest negative correlation of −0.67 to ExG. The inter-correlation among the spectral VIs was mainly due to the similar mathematical operations based on the RGB digital numbers.

4.2. Estimation of H_{canopy} and AGB

The results revealed that the UAV-derived H_{canopy} showed high correlation to the field measurements with the lowest R^2 of 0.72 obtained by the RF model (Table 5). The SWL model achieved the highest accuracy among the three models with a R^2 of 0.88 (RMSE = 0.16 m, rRMSE = 6.40%). After the forward and backward selections with a branch-and-bound algorithm, a subset of UAV variables with higher adjusted R^2 and BIC was obtained, namely, H_{mean}, H_{90}, H_{50} and ExG (Fig. 3a and b). The selected four variables contributed significantly to the SWL model especially H_{mean} and H_{90} ($p < 0.001$) (Table 6). Fig. 4a shows that H_{mean} and H_{90} were the two major predictors for the RF model because both the IncMSE and IncNodePurity were significantly higher than for the other two variables (H_{50}, ExG). Compared with the two parametric models, the RF model showed a weaker performance in the H_{canopy} estimation (RMSE = 0.26 m, rRMSE = 10.40%). Nevertheless, the estimation models for H_{canopy} generally showed a higher robustness than those for AGB with a much lower rRMSE. The estimation accuracies indicated that UAV stereo images can obtain comparable and even higher accuracy in the estimation of maize H_{canopy} compared with ALS data used in other studies, where similar SLR models were employed (Li et al., 2015a). However, slight overestimation still occurred in the low level of canopy height as indicated by the deviation of the fitted line from the 1:1 line in Fig. 5(a).

Different from the H_{canopy} estimation, RF model achieved the best accuracy among the three models in the AGB estimation and successfully explained 78% of the variance of field-measured AGB. The SLR model developed by H_{mean} showed the weakest performance ($R^2 = 0.52$, rRMSE = 18.79%). Fig. 3(c) and (d) shows that H_{mean} obtained the highest frequency to be selected by the SWL models, followed by ExG, H_{cv}, and NGRDI with higher adjusted R^2 and BIC. The two least selected variables were CIVE and WI. The SWL model with the best explaining power ($R^2 = 0.64$, rRMSE = 21.11%) was finally chosen as a linear combination of two spectral VIs and three SfM point metrics (Table 6). All the five UAV variables significantly contributed to the SWL model ($p < 0.05$). Among these variables, ExG contributed the most to the SWL model with a highly significant p value (0.001), followed by H_{mean} ($p = 0.004$). Compared with other variables, H_{cv} showed a weaker but significant contribution to the SWL model with a much higher p value (0.048).

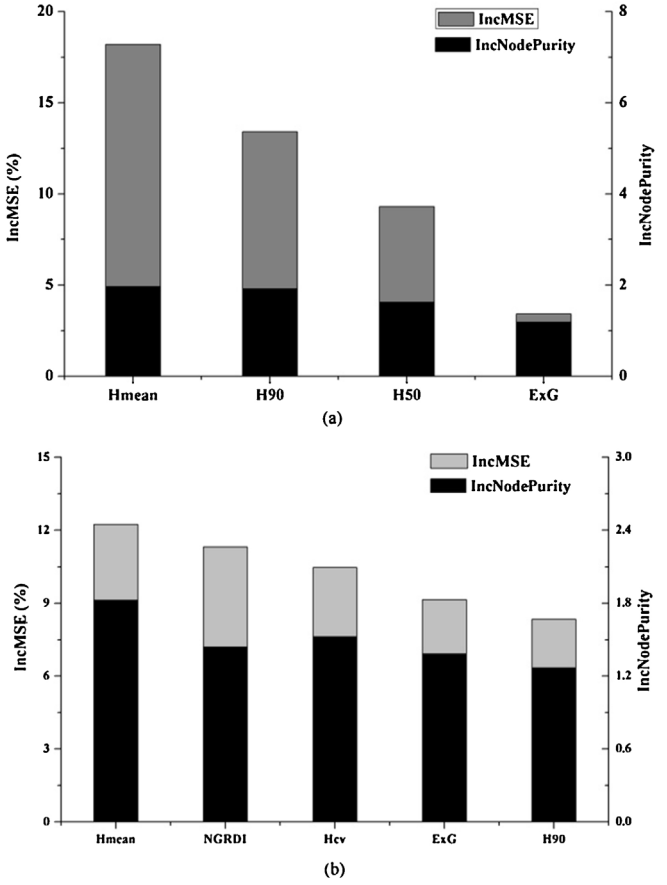

Fig. 4. The selected UAV variables of the RF model for the estimation of (a) H_{canopy} and (b) AGB of maize. The importance of the UAV variables to the model was quantified by percentage increase in mean square error (IncMSE) and total increase in node purities (IncNodePurity).

Table 6
Coefficients and corresponding statistical significance of the stepwise linear regression model (SWL) for estimating the canopy height (H_{canopy}, m) and aboveground biomass of maize (AGB, kg/m^2).

Coefficients	Estimate	p
H_{canopy}		
Intercept	−0.441	0.013
H_{mean}	0.593	<0.001
H_{90}	0.267	<0.001
H_{50}	0.193	0.026
ExG	0.006	0.046
AGB		
Intercept	−1.479	<0.001
H_{mean}	0.329	0.004
ExG	0.019	0.001
NGRDI	4.678	0.014
H_{90}	0.221	0.039
H_{cv}	2.086	0.048

The results showed that the RF model achieved a higher accuracy with a lower ME (0.05) and rRMSE (16.66%), explaining 78% variation of the field-measured AGB. The results showed that the five selected UAV variables all significantly contributed to the RF model with relatively high IncMSE and IncNodePurity (Fig. 5(b)). Specifically, H_{mean} was the most important predictor for the RF model because both the IncMSE and IncNodePurity reached the highest values. NGRDI was the second most important variable with an IncMSE of 11.32% and IncNodePurity of 1.44. The IncMSE for H_{cv} was lower than NGRDI, but its IncNodePurity was slightly higher (1.53 > 1.44). Both ExG and H_{90} showed nearly equivalent contributions to the RF model.

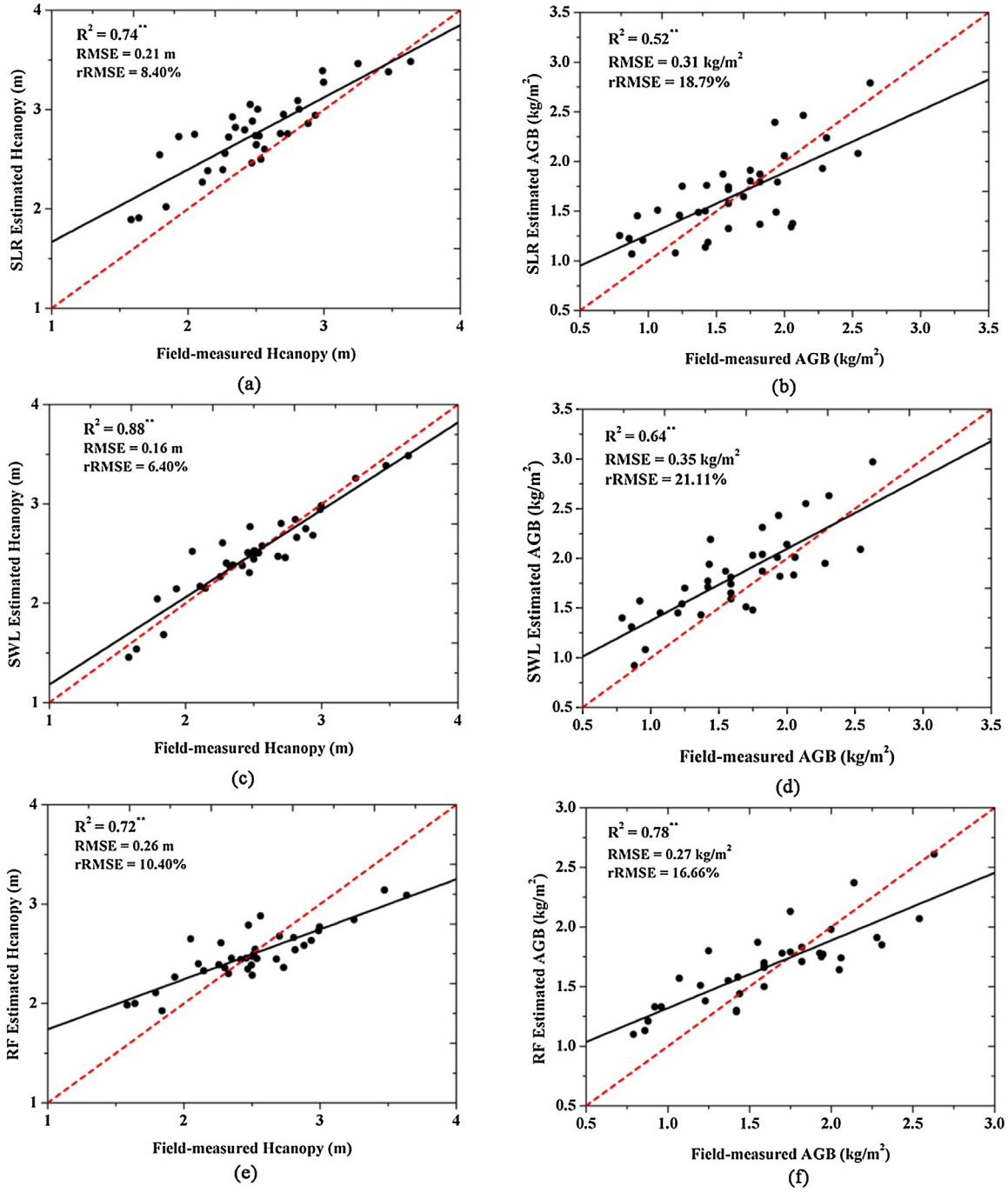

Fig. 5. Comparison of field-measured and UAV-estimated H_{canopy} (m) and AGB (kg/m^2) using (a, b) the SLR model, (c, d) SWL model, and (e, f) RF model. Dashed red line is the 1:1 line. Bold black line is the fitted line. R^2 is the coefficient of determination. $^{**}p < 0.01$. (For interpretation of the references to color in this figure legend, the reader is referred to the web version of the article.)

The one-way ANOVA ($p < 0.05$) results revealed that statistically significant differences were found between the SLR ($M = 2.76$, $SD = 0.39$), SWL ($M = 2.50$, $SD = 0.43$) and RF models ($M = 2.49$, $SD = 0.27$) in the estimation of H_{canopy} (Fig. 6(a)). This indicated that the SLR-estimated H_{canopy} was significantly higher than those estimated by the SWL and RF models. On the other hand, no statistically significant differences were found among the parametric and nonparametric models in the AGB estimation results, as shown in Fig. 6(b). Finally, the SWL model and RF model that achieved the highest model accuracy were applied to the wall-to-wall raster of UAV variables to estimate the spatial distribution of H_{canopy} and AGB, respectively (Fig. 7). The results showed that H_{canopy} in the northeast part of the study site was generally higher than that in the south part. The H_{canopy} for the whole study site obtained an average value of 2.53 m, and a standard deviation of 1.08 m. The AGB showed a different spatial pattern compared with H_{canopy} with a lower level distributed in the northwest part. The northeast part obtained higher levels for both H_{canopy} and AGB. The average and standard deviation of AGB for the study site were 1.75 kg/m^2 and 0.86 kg/m^2, respectively. According to the global statistics, the estimated H_{canopy} (CV = 46.69%) in the study site showed a higher spatial variability than the estimated AGB (CV = 49.14%).

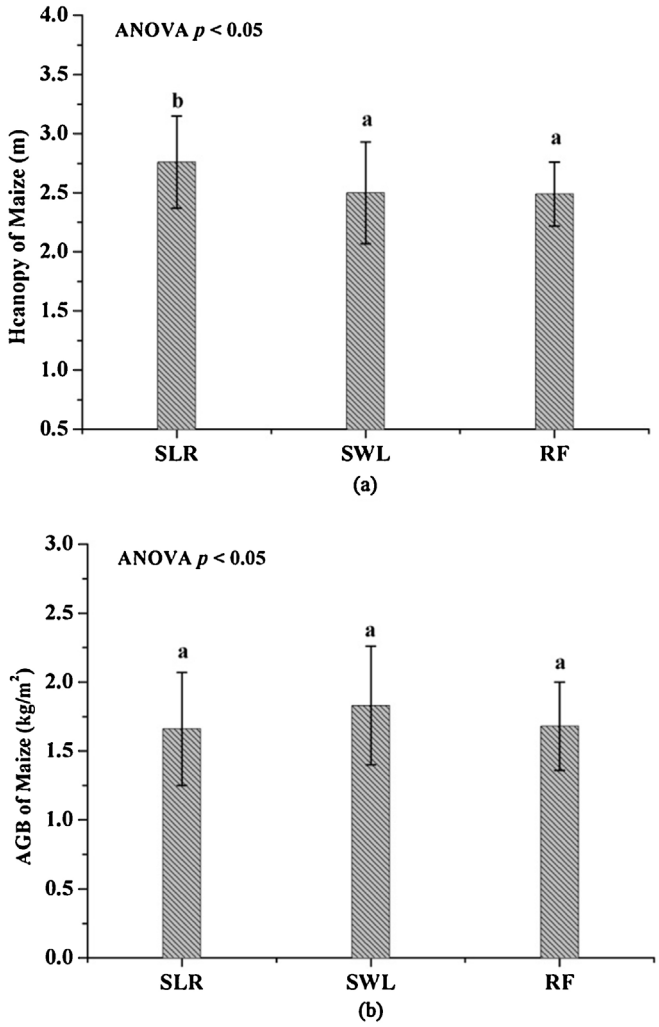

Fig. 6. The statistical significance among the three models (SLR, SWL and RF) for the estimation of (a) H_{canopy} and (b) AGB. The histogram with bars indicated the means ± standard of error. Different letters indicate significant differences at the $p < 0.05$ level, according to one-way ANOVA.

5. Discussion

5.1. UAV-based estimation of maize parameters and uncertainties

Satisfactory results were achieved by estimating the maize H_{canopy} using SfM point variables based on the three regression models in this study. Mean errors of 0.15 m for the SLR model and 0.11 m for the SWL model were obtained, which were comparable and even lower than previous studies, where the H_{canopy} of short vegetation like maize was estimated using ALS data (Jensen and Mathews, 2016; Li et al., 2015a; Luo et al., 2015). The estimated error of H_{canopy} can be explained by different factors. To our knowledge, higher errors tended to exist in the areas near the boundary of the UAV flight due to the lack of sufficient overlapped stereo images. The insufficient stereo images in the boundary part probably increased the variations of the global variability of H_{canopy} and AGB in the whole study area, as higher CVs were obtained for the whole study site than for the field plots. Therefore, it is suggested that repetitive flights should be conducted to obtain a flight area that is larger than the area of interest. In addition, estimation errors might also be caused by the model tuning and manual field measurements with the use of tape. Because only several representative maize plants were measured, measuring errors might exist when the plant stems and top leaves were not fully expanded during the field measurements. In many UAV studies with vegetation, most SfM points come from the canopy surface. However, it is hard to obtain a sufficient number of SfM ground points in areas with highly dense canopies, like the maize field in this study, because the ground is not visible to the passive imaging sensor especially in peak growing season. In this study, the ALS DEM greatly facilitated the employment of SfM point metrics by normalizing the point elevation to the height above ground surface from sea-level. Compared with other studies, our study is unique in employing the same positioning system and flight staff during the ALS and UAV flights, which made it possible to directly use the ALS DEM to normalize the SfM point clouds without registration. In spite of this, the time gap between the UAV and DEM data was likely to bring some errors to the estimation of H_{canopy}. As demonstrated by (Mathews and Jensen, 2013), it is possible to filter sufficient ground points from the SfM point clouds when the vegetation cover is not too dense. Thus, it is recommended to conduct a UAV flight in the early growing season, providing a reliable DEM for the monitoring of canopy height in later seasons.

Previous studies reported that the UAV spectral VIs can be successfully used to estimate the biomass of barley (Bendig et al., 2015). Nevertheless, few studies have employed or compared the ability of UAV SfM point metrics to estimate vegetation biomass for the same dataset. In this study, ALS-similar metrics were calculated from the SfM point clouds to estimate maize AGB together with commonly used spectral VIs. Moderate correlations were found between maize AGB and individual UAV variables, and intercorrelation was found among the UAV variables based on the data collected in this study. Therefore, a possible combination of these predictor variables was explored to improve the model performance. Aasen et al. (2015) suggested that combing multiple UAV predictor variables may improve the estimation accuracy of vegetation parameters, which was supported by this study. The SfM point metrics contributed more to the estimation of maize AGB than the spectral VIs based on our analysis, because three out of the five selected variables were calculated from the SfM point clouds. The sampled spectral VIs generally showed lower spatial variability. This is probably explained by the fact that the data used in this study were collected only on one sampling date. The correlation of VIs to AGB tends to be higher when data collected on more than one date are used because the feature space will be expanded (Aasen et al., 2015). Thus, large spectral variations can be hardly observed by VIs during one sampling date in a relatively small area like the cases in this study. It is likely that multi-temporal UAV and ground measurements can help to improve the feature space contributed from VIs.

In contrast, the UAV height metrics can explain more on the variation of AGB as they can give direct indications to the structure and growing status of the maize canopy. Compared with ALS metrics, SfM point metrics can provide more details on the rugosity and heterogeneity of the canopy surface because of its high point density, while ALS metrics can better describe the structure beneath the canopy surface. Thus, caution should be used that not all of the ALS metrics can be calculated using SfM point clouds. For instance, the commonly used canopy cover/penetration index cannot be calculated using the SfM point clouds in the dense vegetation areas due to the lack of points beneath the canopy surface and through the canopy depth. The SfM H_{mean} was proved to be the most important variable in the RF model, which agrees well with the fact that maize AGB is a height-driven parameter. The high rank obtained by NGRDI and H_{cv} in the AGB estimation model indicated that the horizontal and vertical heterogeneity of the maize canopy can also shed light on the maize AGB. Our previous studies showed that H_{cv} calculated from the ALS point clouds can give an efficient indication of the distribution of forest canopy biomass components

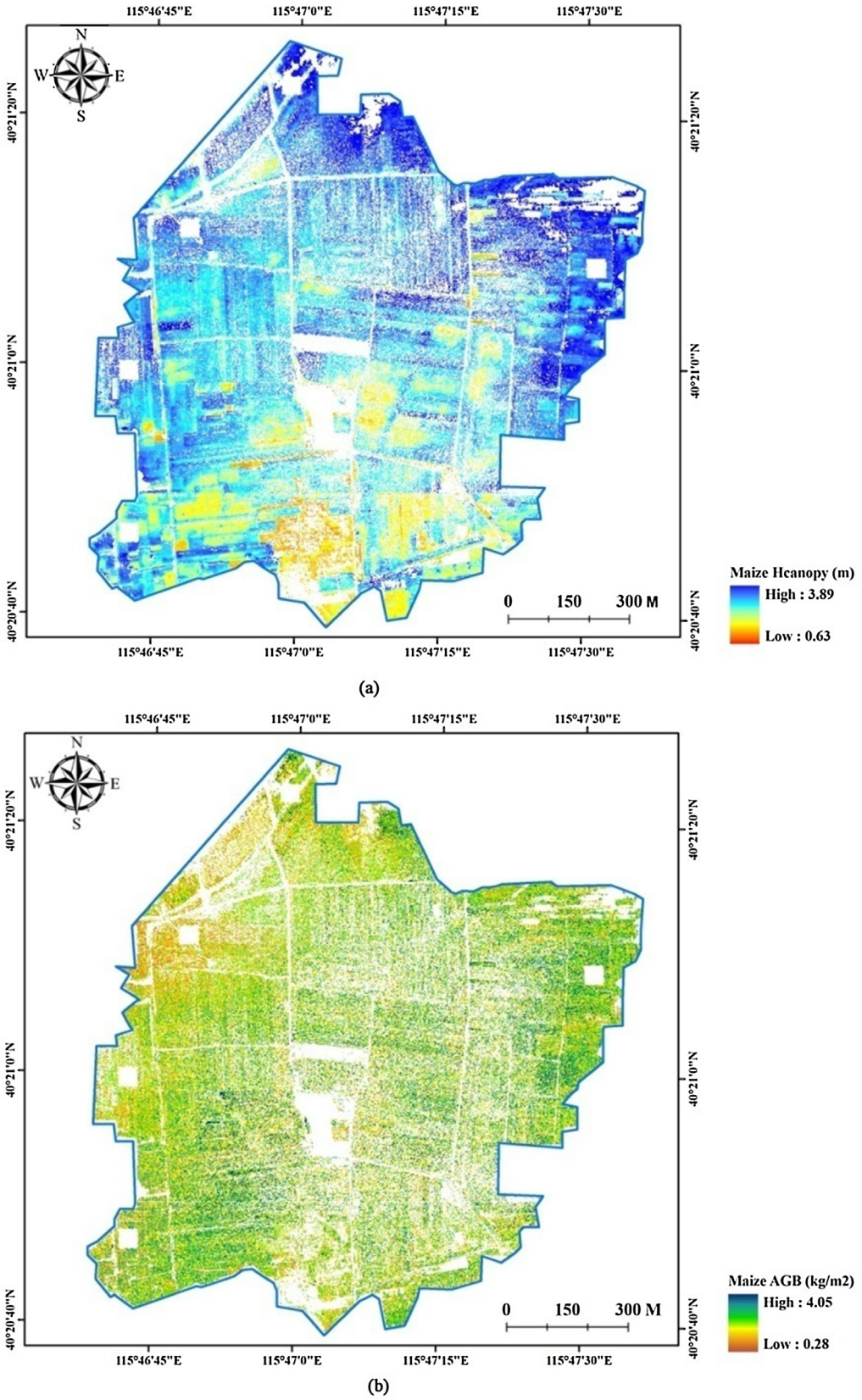

Fig. 7. The spatial pattern of (a) H_{canopy} estimated by SWL model, and (b) AGB estimated by RF model in the maize fields.

(Li et al., 2014). The contribution of H_{cv} to the maize AGB further supported that H_{cv} is also suitable for estimating short vegetation biomass like maize. The high contribution from ExG further supported previous studies that ExG derived from the UAV RGB space can perform well in the estimation of maize AGB aside from the vegetation fraction of wheat (Torres-Sánchez et al., 2014). Overall, the simultaneous selection of both spectral VIs and SfM point metrics by the estimation models of AGB indicated that the variations in spectral and structural attributes for the maize canopy should be simultaneously considered when only simple RGB images are available for estimating maize AGB in future. In addition, the UAV flight specifications such as flight height, field of view, image resolution changes, and image overlap may also influence the estimation of maize parameters, which should be investigated in future studies.

5.2. Limitations and implications of this study

Satisfactory results were obtained on the estimation of maize H_{canopy} and AGB based on the UAV data collected in this study. The addition of the SfM point metrics produced from the stereo images further enriched the previous studies on remote monitoring of maize parameters. Nevertheless, most SfM point clouds come from the canopy surface and are limited in providing more detail on the spectral and structural variations within deep canopies. In contrast, ALS and TLS can provide detailed structural variations along the canopy depth while they can hardly provide sufficient spectral characteristics. With the development of remote sensors, UAV laser scanning will be a very promising alternative to supplement the stereo images in the long-term monitoring of crops, which has been initially tested in the application of forest inventory (Wallace et al., 2012a,b). In addition, the full-waveform laser scanning system mounted on the UAV will greatly improve the layered detection of biophysical and biochemical variations in crop canopies. Future efforts can be used to combine the data collected by these two UAV sensors in precision agro-ecological studies. On the other hand, the classification accuracy for maize at the study site could not be quantitatively evaluated, limited by the insufficiently large sample size. In this study, we believed that the classification map was reasonable because the land cover in this study site is mainly dominated by obvious block maize fields. In addition, the remotely sensed characteristics of maize field were evident and can be easily discriminated from other land cover types, and all the 37 plots were located in the maize classification map.

In this study, all of the spectral variables were calculated from the RGB space of orthorectified image due to the use of simple CCD cameras. In fact, more diverse spectral characteristics can be obtained when a hyperspectral camera is loaded on the UAV system (Duan et al., 2014; Hruska et al., 2012), which can greatly broaden the estimation of maize parameters including AGB (Honkavaara et al., 2013). The estimation models and application scope will also vary significantly when more data from UAV laser scanning and hyperspectral camera are available. In addition, the intercorrelation among the spectral predictor variables that occurred in this study will be reduced as more VIs can be calculated and selected from the hyperspectral data. With the UAV hyperspectral data, precision classification of vegetation and estimates of biochemical parameters can be conducted by making use of the spectral information. In the aspect of operability and accessibility, UAV-based data can be collected exactly when they are needed compared with the satellite-based remote sensing data. This is of great importance for the long-term detection of crops, because the growing status of crops varies among different growing seasons. Furthermore, the very high resolution of UAV data makes it more suitable for small and medium level applications like precision agriculture, providing basic materials for applications at regional and global scales.

6. Conclusion

In this study, hundreds of stereo images with very high resolution were collected by a low-cost UAV system, which were further applied to the estimation of maize H_{canopy} and AGB. In addition, the commonly used spectral VIs, ALS-similar metrics calculated from the UAV SfM point clouds were also tested in the estimation of maize parameters for the first time. The results showed that the UAV-estimated maize parameters were comparable to the field measurements with a mean error of 0.11 m for H_{canopy}, and 0.05 kg/m^2 for AGB. The SfM point metrics, especially H_{mean} greatly contributed to the estimation model of maize AGB, which can be promising indicators in the detection of maize biophysical parameters. To conclude, the variations in spectral and structural attributes for maize canopy should be simultaneously considered when only simple RGB images are available for estimating maize AGB in future. This provides some suggestions on how to make full use of the low-cost and high-resolution UAV stereo images in precision agro-ecological applications and management.

Acknowledgements

This work was supported by the Open Research Fund of Key Laboratory of Digital Earth Science, Chinese Academy of Sciences (2014LDE008); National Natural Science Foundation of China (41401399); China's Special Funds for Major State Basic Research Project of China (2013CB733405); and the National High Technology Research and Development Program of China (863 Program) (2014AA06A511); the Special Foundation for Young Scientists from the director of the Institute of Remote Sensing and Digital Earth, Chinese Academy of Sciences.

References

Aasen, H., Burkart, A., Bolten, A., Bareth, G., 2015. Generating 3D hyperspectral information with lightweight UAV snapshot cameras for vegetation monitoring: from camera calibration to quality assurance. ISPRS J. Photogram. Rem. Sens. 108, 245–259, http://dx.doi.org/10.1016/j.isprsjprs.2015.08.002.

Becker-Reshef, I., Vermote, E., Lindeman, M., Justice, C., 2010. A generalized regression-based model for forecasting winter wheat yields in Kansas and Ukraine using MODIS data. Rem. Sens. Environ. 114, 1312–1323, http://dx.doi.org/10.1016/j.rse.2010.01.010.

Bendig, J., Yu, K., Aasen, H., Bolten, A., Bennertz, S., Broscheit, J., Gnyp, M.L., Bareth, G., 2015. Combining UAV-based plant height from crop surface models, visible, and near infrared vegetation indices for biomass monitoring in barley. Int. J. Appl. Earth Observ. Geoinf. 39, 79–87, http://dx.doi.org/10.1016/j.jag.2015.02.012.

Candiago, S., Remondino, F., De Giglio, M., Dubbini, M., Gattelli, M., 2015. Evaluating multispectral images and vegetation indices for precision farming applications from UAV images. Rem. Sens. 7, 4026–4047, http://dx.doi.org/10.3390/rs70404026.

Colomina, I., Molina, P., 2014. Unmanned aerial systems for photogrammetry and remote sensing: a review. ISPRS J. Photogram. Rem. Sens. 92, 79–97, http://dx.doi.org/10.1016/j.isprsjprs.2014.02.013.

Coltri, P.P., Zullo Jr., J., do Valle Goncalves, R.R., Romani, L.A.S., Pinto, H.S., 2013. Coffee crop's biomass and carbon stock estimation with usage of high resolutionsatellites images. IEEE J. Sel. Top. Appl. Earth Observ. Rem. Sens. 6, 1786–1795, http://dx.doi.org/10.1109/jstars.2013.2262767.

Duan, S.-B., Li, Z.-L., Wu, H., Tang, B.-H., Ma, L., Zhao, E., Li, C., 2014. Inversion of the PROSAIL model to estimate leaf area index of maize, potato, and sunflower fields from unmanned aerial vehicle hyperspectral data. Int. J. Appl. Earth Observ. Geoinf. 26, 12–20, http://dx.doi.org/10.1016/j.jag.2013.05.007.

Gao, S., Niu, Z., Huang, N., Hou, X., 2013. Estimating the leaf area index, height and biomass of maize using HJ-1 and RADARSAT-2. Int. J. Appl. Earth Observ. Geoinf. 24, 1–8, http://dx.doi.org/10.1016/j.jag.2013.02.002.

Gao, S., Niu, Z., Sun, G., Zhao, D., Jia, K., Qin, Y., 2015. Height extraction of maize using aiborne full-waveform LiDAR data and a deconvolution algorithm. IEEE Geosci. Rem. Sens. Lett. 12, 1978–1982, http://dx.doi.org/10.1109/LGRS.2015.2441655.

Geipel, J., Link, J., Claupein, W., 2014. Combined spectral and spatial modeling of corn yield based on aerial images and crop surface models acquired with an Unmanned Aircraft System. Rem. Sens. 6, 10335–10355, http://dx.doi.org/10.3390/rs61110335.

Getzin, S., Nuske, R., Wiegand, K., 2014. Using Unmanned Aerial Vehicles (UAV) to quantify spatial gap patterns in forests. Rem. Sens. 6, 6988–7004, http://dx.doi.org/10.3390/rs6086988.

Gitelson, A.A., Kaufman, Y.J., Stark, R., Rundquist, D., 2002. Novel algorithms for remote estimation of vegetation fraction. Rem. Sens. Environ. 80, 76–87, http://dx.doi.org/10.1016/S0034-4257(01)00289-9.

Gonsamo, A., 2010. Leaf area index retrieval using gap fractions obtained from high resolution satellite data: comparisons of approaches, scales and atmospheric effects. Int. J. Appl. Earth Observ. Geoinf. 12, 233–248, http://dx.doi.org/10.1016/j.jag.2010.03.002.

Gonsamo, A., Chen, J.M., D'Odorico, P., 2013. Deriving land surface phenology indicators from CO_2 eddy covariance measurements. Ecol. Indic. 29, 203–207, http://dx.doi.org/10.1016/j.ecolind.2012.12.026.

Guijarro, M., Pajares, G., Riomoros, I., Herrera, P.J., Burgos-Artizzu, X.P., Ribeiro, A., 2011. Automatic segmentation of relevant textures in agricultural images. Comput. Electron. Agric. 75, 75–83, http://dx.doi.org/10.1016/j.compag.2010.09.013.

Höfle, B., 2014. Radiometric correction of terrestrial LiDAR point cloud data for individual maize plant detection. IEEE Geosci. Rem. Sens. Lett. 11, 94–98, http://dx.doi.org/10.1109/lgrs.2013.2247022.

Höfle, B., Hollaus, M., Hagenauer, J., 2012. Urban vegetation detection using radiometrically calibrated small-footprint full-waveform airborne LiDAR data. ISPRS J. Photogram. Rem. Sens. 67, 134–147, http://dx.doi.org/10.1016/j.isprsjprs.2011.12.003.

Hague, T., Tillett, N.D., Wheeler, H., 2006. Automated crop and weed monitoring in widely spaced cereals. Precis. Agric. 7, 21–32, http://dx.doi.org/10.1007/s11119-005-6787-1.

Honkavaara, E., Saari, H., Kaivosoja, J., Pölönen, I., Hakala, T., Litkey, P., Mäkynen, J., Pesonen, L., 2013. Processing and assessment of spectrometric, stereoscopic imagery collected using a lightweight UAV spectral camera for precision agriculture. Rem. Sens. 5, 5006–5039, http://dx.doi.org/10.3390/rs5105006.

Hruska, R., Mitchell, J., Anderson, M., Glenn, N.F., 2012. Radiometric and geometric analysis of hyperspectral imagery acquired from an Unmanned Aerial Vehicle. Rem. Sens. 4, 2736–2752, http://dx.doi.org/10.3390/rs4092736.

Hyyppa, J., Yu, X.W., Hyyppa, H., Vastaranta, M., Holopainen, M., Kukko, A., Kaartinen, H., Jaakkola, A., Vaaja, M., Koskinen, J., Alho, P., 2012. Advances in forest inventory using airborne laser scanning. Rem. Sens. 4, 1190–1207, http://dx.doi.org/10.3390/rs4051190.

Jaakkola, A., Hyyppä, J., Kukko, A., Yu, X., Kaartinen, H., Lehtomäki, M., Lin, Y., 2010. A low-cost multi-sensoral mobile mapping system and its feasibility for tree measurements. ISPRS J. Photogram. Rem. Sens. 65, 514–522, http://dx.doi.org/10.1016/j.isprsjprs.2010.08.002.

Jensen, J., Mathews, A., 2016. Assessment of image-based point cloud products to generate a bare earth surface and estimate canopy heights in a woodland ecosystem. Rem. Sens. 8, 50, http://dx.doi.org/10.3390/rs8010050.

Kataoka, T., Kaneko, T., Okamoto, H., 2003. Crop growth estimation system using machine vision. In: Advanced Intelligent Mechatronics, 2003. AIM 2003. Proceedings. 2003 IEEE/ASME International Conference on. IEEE. vol. 1072, pp. b1079–b1083.

Kross, A., McNairn, H., Lapen, D., Sunohara, M., Champagne, C., 2015. Assessment of RapidEye vegetation indices for estimation of leaf area index and biomass in corn and soybean crops. Int. J. Appl. Earth Observ. Geoinf. 34, 235–248, http://dx.doi.org/10.1016/j.jag.2014.08.002.

Leberl, F., Irschara, A., Pock, T., Meixner, P., Gruber, M., Scholz, S., Wiechert, A., 2010. Point clouds: lidar versus 3D vision. Photogramm. Eng. Rem. Sens. 76, 1123–1134.

Li, W., Niu, Z., Gao, S., Huang, N., Chen, H.Y., 2014. Correlating the horizontal and vertical distribution of LiDAR point clouds with components of biomass in a Picea crassifolia forest. Forests 5, 1910–1930, http://dx.doi.org/10.3390/f5081910.

Li, W., Niu, Z., Huang, N., Wang, C., Gao, S., Wu, C., 2015a. Airborne LiDAR technique for estimating biomass components of maize: a case study in Zhangye City, Northwest China. Ecol. Indic. 57, 486–496, http://dx.doi.org/10.1016/j.ecolind.2015.04.016.

Li, W., Niu, Z., Liang, X., Li, Z., Huang, N., Gao, S., Wang, C., Muhammad, S., 2015b. Geostatistical modeling using LiDAR-derived prior knowledge with SPOT-6 data to estimate temperate forest canopy cover and above-ground biomass via stratified random sampling. Int. J. Appl. Earth Observ. Geoinf. 41, 88–98, http://dx.doi.org/10.1016/j.jag.2015.04.020.

Li, W., Niu, Z., Wang, C., Huang, W., Chen, H., Gao, S., Li, D., Muhammad, S., 2015c. Combined use of airborne LiDAR and satellite GF-1 data to estimate leaf area index, height, and aboveground biomass of maize during peak growing season. IEEE J. Sel. Top. Appl. Earth Observ. Rem. Sens. 9, 4489–4501.

Liebisch, F., Kirchgessner, N., Schneider, D., Walter, A., Hund, A., 2015. Remote, aerial phenotyping of maize traits with a mobile multi-sensor approach. Plant Methods 11, http://dx.doi.org/10.1186/s13007-015-0048-8.

Link, J., Senner, D., Claupein, W., 2013. Developing and evaluating an aerial sensor platform (ASP) to collect multispectral data for deriving management decisions in precision farming. Comput. Electron. Agric. 94, 20–28, http://dx.doi.org/10.1016/j.compag.2013.03.003.

Lisein, J., Pierrot-Deseilligny, M., Bonnet, S., Lejeune, P., 2013. A photogrammetric workflow for the creation of a forest canopy height model from small unmanned aerial system imagery. Forests 4, 922–944, http://dx.doi.org/10.3390/f4040922.

Listopad, C.M.C.S., Masters, R.E., Drake, J., Weishampel, J., Branquinho, C., 2015. Structural diversity indices based on airborne LiDAR as ecological indicators for managing highly dynamic landscapes. Ecol. Indic. 57, 268–279, http://dx.doi.org/10.1016/j.ecolind.2015.04.017.

Liu, J., Pattey, E., Miller, J.R., McNairn, H., Smith, A., Hu, B., 2010. Estimating crop stresses, aboveground dry biomass and yield of corn using multi-temporal optical data combined with a radiation use efficiency model. Rem. Sens. Environ. 114, 1167–1177, http://dx.doi.org/10.1016/j.rse.2010.01.004.

Louhaichi, M., Borman, M.M., Johnson, D.E., 2001. Spatially located platform and aerial photography for documentation of grazing impacts on wheat. Geocarto Int. 16, 65–70.

Luo, S., Wang, C., Pan, F., Xi, X., Li, G., Nie, S., Xia, S., 2015. Estimation of wetland vegetation height and leaf area index using airborne laser scanning data. Ecol. Indic. 48, 550–559, http://dx.doi.org/10.1016/j.ecolind.2014.09.024.

Mathews, A., Jensen, J., 2013. Visualizing and quantifying vineyard canopy LAI using an unmanned aerial vehicle (UAV) collected high density structure from motion point cloud. Rem. Sens. 5, 2164–2183, http://dx.doi.org/10.3390/rs5052164.

Neto, J.C., 2004. A combined statistical-soft computing approach for classification and mapping weed species in minimum-tillage systems. In: ETD Collection for University of Nebraska – Lincoln., pp. 1–170.

Ni, W., Ranson, K.J., Zhang, Z., Sun, G., 2014. Features of point clouds synthesized from multi-view ALOS/PRISM data and comparisons with LiDAR data in forested areas. Rem. Sens. Environ. 149, 47–57, http://dx.doi.org/10.1016/j.rse.2014.04.001.

Ni, W., Sun, G., Ranson, K.J., Pang, Y., Zhang, Z., Yao, W., 2015. Extraction of ground surface elevation from ZY-3 winter stereo imagery over deciduous forested areas. Rem. Sens. Environ. 159, 194–202, http://dx.doi.org/10.1016/j.rse.2014.12.007.

Nie, S., Wang, C., Dong, P., Xi, X., 2016. Estimating leaf area index of maize using airborne full-waveform lidar data. Rem. Sens. Lett. 7, 111–120, http://dx.doi.org/10.1080/2150704x.2015.1111536.

Omasa, K., Hosoi, F., Konishi, A., 2007. 3D lidar imaging for detecting and understanding plant responses and canopy structure. J. Exp. Bot. 58, 881–898.

Pang, Y., Li, Z.-Y., 2013. Inversion of biomass components of the temperate forest using airborne Lidar technology in Xiaoxing'an Mountains, Northeastern of China. Chin. J. Plant Ecol. 36, 1095–1105.

Pena, J.M., Torres-Sanchez, J., de Castro, A.I., Kelly, M., Lopez-Granados, F., 2013. Weed mapping in early-season maize fields using object-based analysis of unmanned aerial vehicle (UAV) images. PLOS ONE 8, e77151, http://dx.doi.org/10.1371/journal.pone.0077151.

Tian, X., Li, Z., Su, Z., Chen, E., van der Tol, C., Li, X., Guo, Y., Li, L., Ling, F., 2014. Estimating montane forest above-ground biomass in the upper reaches of the Heihe River Basin using Landsat-TM data. Int. J. Rem. Sens. 35, 7339–7362, http://dx.doi.org/10.1080/01431161.2014.967888.

Torres-Sánchez, J., Peña, J.M., de Castro, A.I., López-Granados, F., 2014. Multi-temporal mapping of the vegetation fraction in early-season wheat fields using images from UAV. Comput. Electron. Agric. 103, 104–113, http://dx.doi.org/10.1016/j.compag.2014.02.009.

Wallace, L., Lucieer, A., Watson, C., Turner, C., 2012a. Assessing the feasibility of UAV-based LiDAR for high resolution forest change detection. Proc. ISPRS—Int. Archives Photogramm., Rem. Sens. Spatial Inf. Sci. 39, B7.

Wallace, L., Lucieer, A., Watson, C., Turner, D., 2012b. Development of a UAV-LiDAR system with application to forest inventory. Rem. Sens. 4, 1519–1543, http://dx.doi.org/10.3390/rs4061519.

White, J., Wulder, M., Vastaranta, M., Coops, N., Pitt, D., Woods, M., 2013. The utility of image-based point clouds for forest inventory: a comparison with airborne laser scanning. Forests 4, 518–536, http://dx.doi.org/10.3390/f4030518.

Woebbecke, D., Meyer, G., Von Bargen, K., Mortensen, D., 1995. Color indices for weed identification under various soil, residue, and lighting conditions. Trans. ASAE 38, 259–269.

Wu, C.Y., Chen, J.M., 2013. Deriving a new phenological indicator of interannual net carbon exchange in contrasting boreal deciduous and evergreen forests. Ecol. Indic. 24, 113–119, http://dx.doi.org/10.1016/j.ecolind.2012.06.006.

Wu, C.Y., Niu, Z., Gao, S., 2012. The potential of the satellite derived green chlorophyll index for estimating midday light use efficiency in maize, coniferous forest and grassland. Ecol. Indic. 14, 66–73, http://dx.doi.org/10.1016/j.ecolind.2011.08.018.

Wu, C.Y., Niu, Z., Tang, Q., Huang, W.J., 2008. Estimating chlorophyll content from hyperspectral vegetation indices: modeling and validation. Agric. Forest Meteorol. 148, 1230–1241, http://dx.doi.org/10.1016/j.agrformet.2008.03.005.

Zaman-Allah, M., Vergara, O., Araus, J.L., Tarekegne, A., Magorokosho, C., Zarco-Tejada, P.J., Hornero, A., Hernandez Alba, A., Das, B., Craufurd, P., Olsen, M., Prasanna, B.M., Cairns, J., 2015. Unmanned aerial platform-based multi-spectral imaging for field phenotyping of maize. Plant Methods 11, http://dx.doi.org/10.1186/s13007-015-0078-2.